Depletion interactions of non-spherical colloidal particles in polymer solutions

E Eisenriegler and A Bringer

Institut für Festkörperforschung, Forschungszentrum Jülich, D-52425 Jülich, Germany

Abstract
We consider anisotropic colloidal particles immersed in a solution of long, flexible, and non-adsorbing polymers. For the dumbbell shapes of recently synthesized particles consisting of two intersecting spheres, and for lens-shaped particles with spherical surfaces, we calculate the isotropic and anisotropic interaction parameters that determine the immersion free energy and the orientation-dependent depletion interaction between particles that are induced by the polymers. Exact results are obtained for ideal (random walk) polymer chains.

(Some figures in this article are in colour only in the electronic version)

1. Introduction

In colloidal suspensions containing polymer chains, there are tunable effective interactions between the colloid particles. Free non-adsorbing polymer chains avoid the space between two particles, leading to an unbalanced pressure, which pushes them towards each other. Such depletion forces for an isolated pair of immersed particles or for a single immersed particle near a wall have been measured in recent experiments [1].

Here we consider *anisotropic* colloid particles. For the dumbbell shapes of recently synthesized [2] particles consisting of two intersecting spheres, and for lens-shaped particles with spherical surfaces, as in figure 1, we calculate the immersion free energy and the *orientation-dependent* depletion interaction. The predictions are compared with results for prolate and oblate ellipsoids [3–5], which also have a symmetry axis of revolution and a symmetry centre of reflection.

The case of *large* particle to polymer size ratio can be investigated by means of small curvature expansions of the Helfrich or Derjaguin type, but here we consider mesoscopic particles which are *small* compared to characteristic polymer lengths such as the gyration radius $\mathcal{R}_g$, and we concentrate on the case of *ideal*, random walk, polymers. The well known correspondence [6] between the statistics of long flexible polymers and critical field theories allows us to use the *small particle operator expansion* [7–9] for predicting the polymer-induced
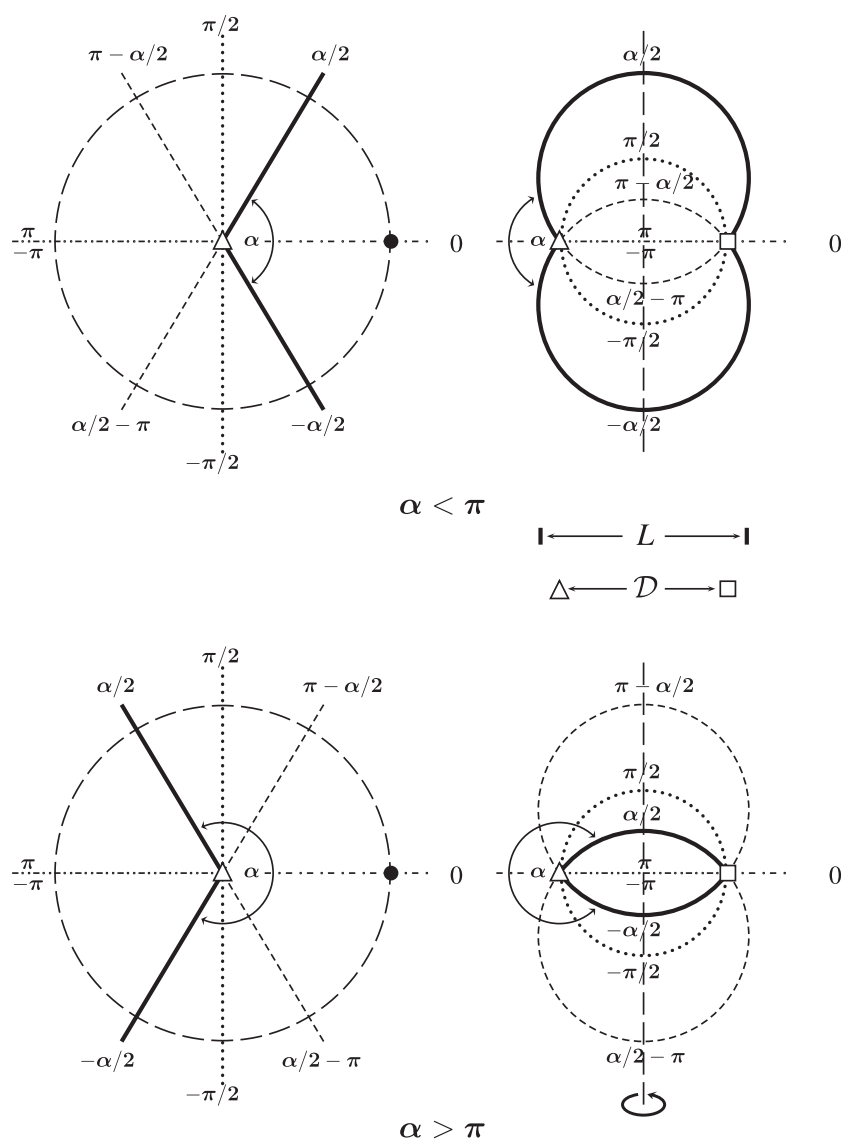
Figure 1. Conformal mapping of a wedge onto a dumbbell or lens.

interactions. The operator weights in the expansion for dumbbells and lenses are calculated by a conformal mapping to a wedge geometry.

We introduce the polymer–magnet analogy and small particle expansion in section 2, discuss density profiles in a wedge and outside a dumbbell or lens in section 3, and evaluate, for ideal polymers, the corresponding small particle amplitudes in the Gaussian model in section 4. These results are compared with corresponding results for ellipsoids and, in section 5, with a more general class of weakly anisotropic particles. In section 6 the amplitudes are used to determine the orientation-dependent interactions, and in section 7 we summarize the new results. Some technical details are relegated to appendices A–D.

2. Polymer–magnet analogy and small particle expansion

In the polymer–magnet analogy the partition function of a polymer chain with ends at r_1 and r_2 corresponds to the order parameter correlation function $\langle \varphi_{12} \rangle$ of a Ginzburg–Landau model or field theory [5, 6]. Here φ_{12} is the product $\Phi(r_1)\Phi(r_2)$ of two order parameter fields Φ. *Ideal* polymers correspond to a *Gaussian* Ginzburg–Landau model with Hamiltonian

$$H = \int \mathrm{d}r \left[\frac{1}{2}(\nabla\Phi)^2 + \frac{t}{2}\Phi^2 \right], \tag{2.1}$$

where the integration extends over the volume outside the particles, and where the order parameter satisfies the Dirichlet boundary condition

$$\Phi = 0 \tag{2.2}$$

at the particle surfaces, since we consider non-adsorbing polymers. We always consider length scales much larger than the persistence and extrapolation lengths.

  The free energy F it costs to immerse particles in a dilute polymer solution in an unbounded space or in the half space bounded by a wall is determined by the polymer partition functions with and without the particles, and is given by [4, 5]

$$F/p_0 = -\mathcal{L} \int \mathrm{d}r_1 \, \mathrm{d}r_2 [\langle\varphi_{12}\rangle_{\mathcal{H}+\delta\mathcal{H}} - \langle\varphi_{12}\rangle_{\mathcal{H}}]. \tag{2.3}$$

Here $p_0 = nk_\mathrm{B}T$ is the ideal gas pressure in the dilute solution with chain density n, and $\mathcal{H}+\delta\mathcal{H}$ and $\mathcal{H}$ denote Ginzburg–Landau Hamiltonians of the form (2.1) in the presence and absence of the particles, respectively. The dependence of the double integral on the temperature deviation t from the critical point is converted into the dependence on $\mathcal{R}_\mathrm{g}^2$ of $-F/p_0$ by means of the inverse Laplace transform $\mathcal{L}(..) = \int (\mathrm{d}t/2\pi\mathrm{i}) \exp(3t\mathcal{R}_\mathrm{g}^2/d)(..)$, where d denotes the spatial dimension.

  Consider particles with a size much smaller than $\mathcal{R}_\mathrm{g}$ and a shape that is symmetric about both a centre of reflection and an axis of revolution. Examples are rods, discs, ellipsoids, dumbbells, and lenses. In the spirit of the operator-product expansion, a small mesoscopic perturbation in a critical field theory can be represented by a sum of point operators. Thus, for a single small particle [7–9][1] with centre at r_P,

$$\mathrm{e}^{-\delta\mathcal{H}} \propto 1 + \sigma_I + \sigma_A, \tag{2.4}$$

where

$$\sigma_I = a_1\epsilon(r_\mathrm{P}) + \cdots, \tag{2.5}$$

$$\sigma_A = b_1\partial_\parallel^2\epsilon(r_\mathrm{P}) + b_2 T_{\parallel\parallel}(r_\mathrm{P}) + \cdots \tag{2.6}$$

are linear combinations of *isotropic (I)* and *anisotropic (A)* operators from the operator algebra of the Ginzburg–Landau model, which reflect the symmetries of the particle shape and boundary condition. Here $\epsilon \propto -\Phi^2$ is the energy density, $\partial_\parallel$ is a derivative along the particle axis, and $T_{\parallel\parallel}$ is the diagonal component of the stress tensor of the field theory along the axis.

  Only the operators of lowest scaling dimensions $x = d - 1/\nu, d + 2 - 1/\nu, d$ are shown in equations (2.4)–(2.6), and their coefficients a_1, b_1, b_2 by scale invariance must be

---

[1] First, equation (2.4) applies to correlation functions with operators much further away from r_P than the particle size. Apart from contact terms [4], equation (2.4) may also be used for calculating integrals such as (2.3). Here we only consider the leading isotropic and anisotropic contributions for small particle size, and the contact terms do not contribute. The leading contact term has particle size exponent d and is isotropic [4].

proportional to the particle size raised to the power x. For ideal chains (Gaussian model) the Flory (correlation length) exponent ν equals $1/2$, so that $\partial_\parallel^2 \epsilon$ and $T_{\parallel\parallel}$ have the same scaling dimension d, and the b_1 and b_2 terms both contribute to the leading anisotropic behaviour. For chains with excluded volume interaction (corresponding [6] to the N-vector model in the limit $N \to 0$), ν is larger than $1/2$, and we expect that the b_2 term dominates the anisotropic behaviour of a small particle.

The coefficients a_1, b_1, b_2 depend on the size and shape of the particle but are *independent* of other distant particles, of the distant boundary wall of the half space, and[2] of t. Thus we evaluate the coefficients for a *single* particle in an *unbounded* space at $t = 0$, and then use them to make predictions for the interaction between particles or a particle and a wall. The coefficients can be evaluated from the density profiles $\langle \epsilon(r) \rangle$ and $\langle T_{kl}(r) \rangle$ of the energy density and the stress tensor that are induced by a single particle. While ellipsoids have been considered in [4, 5] we concentrate here on dumbbells and lens-shaped particles.

3. Densities in a wedge and outside a dumbbell or lens

A system at the critical point containing a colloidal dumbbell composed of two overlapping spheres, or a lens with two spherical surfaces, can be conformally mapped onto a critical system filling a wedge with opening angle α, which is smaller or larger than π in case of the dumbbell or lens, as in figure 1. As explained in more detail in [9], an inversion about the point denoted by the heavy dot on the left-hand side of figure 1 maps the interior of the wedge onto the exterior of a particle with a dumbbell or lens shape. The two boundary half planes of the wedge and the edge where they meet are mapped onto the two spherical surfaces of the particle and the circle C of diameter $\mathcal{D}$ where they intersect. $\mathcal{D}$ is related to the diameter L of the two spheres by $\mathcal{D} = L \sin(\alpha/2)$. For $\alpha = 0, \pi$, and 2π the particle on the right-hand side of figure 1 becomes a dumbbell of two touching spheres, a spherical particle, and a circular disc, respectively.

For the wedge the boundary-induced density profile of a scalar operator $\mathcal{O}$, such as the energy density ϵ, has the form [10–12]

$$\langle \mathcal{O}(\hat{r}_e, \rho, \Omega) \rangle_{\text{wedge}}^{(i,j)} = B_\mathcal{O}^{1/2} \rho^{-x_\mathcal{O}} \bar{\mathcal{P}}_{i,j}(\alpha, \Omega). \tag{3.1}$$

Here the position vector $\hat{r}$ is expressed in cylindrical coordinates $(\hat{r}_e, \rho, \Omega)$, where the edge of the wedge is the axis. The component $\hat{r}_e$ is parallel to the edge (and in general has dimension $d - 2$), and the two-component vector perpendicular to the edge is determined by its angle Ω with the symmetry half plane of the wedge, i.e. $-\alpha/2 \leqslant \Omega \leqslant \alpha/2$, and by the distance ρ from the edge. While $\bar{\mathcal{P}}$ is a universal scaling function, $B_\mathcal{O}$ is the non-universal amplitude in the pair correlation function

$$\langle \mathcal{O}(r) \mathcal{O}(0) \rangle_{\text{bulk}} = B_\mathcal{O} r^{-2x_\mathcal{O}} \tag{3.2}$$

of $\mathcal{O}$ in the bulk. The indices (i, j) characterize the surface universality classes[3] of the two boundary half planes $\Omega = (-\alpha/2, \alpha/2)$ of the wedge.

The corresponding density $\langle \mathcal{O}(r) \rangle_{\text{particle}}$ outside a dumbbell or lens follows [10] from (3.1) and the conformal mapping and has the form given in equations (5.14) and (5.10) of [9]. Turning

---

[2] Compare the discussion in [4, 5] for the Gaussian model. In the notation of [5] with amplitudes β in equations (162)–(165), $a_1\sqrt{B_\epsilon} = \beta_\text{I} \tilde{S}_d/\sqrt{2}$, $b_1\sqrt{B_\epsilon} = (\beta_\text{VI}(d-2) + \beta_\text{VII}d)\tilde{S}_d/(4\sqrt{2}(d-1))$, $b_2 = (-\beta_\text{VI} + \beta_\text{VII})/2$ with $\tilde{S}_d$ given in (4.1).

[3] While we concentrate in sections 4–6 on non-adsorbing ideal chains represented by the Gaussian model with Dirichlet boundary conditions, the discussion in section 3 does not specify the bulk and surface universality classes [10] and allows also for other applications [9, 12].
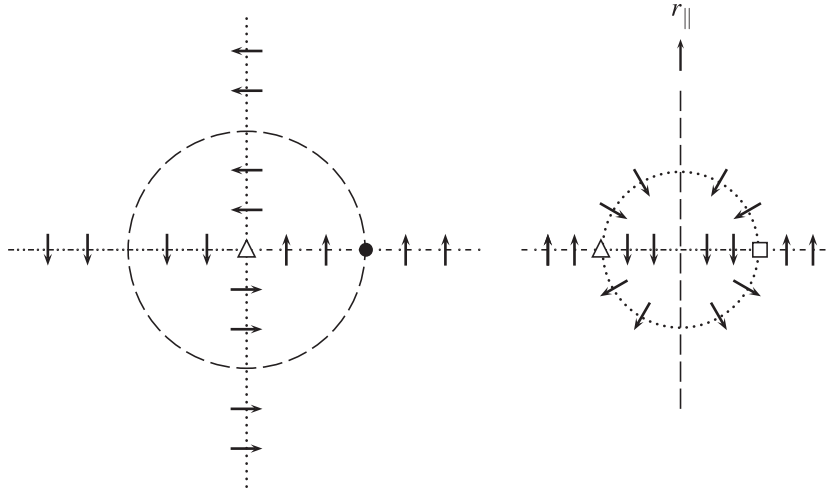
Figure 2. The normalized eigenvectors $u^{(n)}(\Omega)$ (left) and $u^{(N)}(r)$ (right) of the stress tensor density in a wedge and outside a dumbbell or lens. The vector field $u^{(N)}$ is determined by equation (3.10). The symbols for lines and points correspond to those in figure 1.

to the energy density $\mathcal{O} = \epsilon$ with scaling function $\bar{\mathcal{P}} = \bar{\mathcal{E}}$ and equal boundaries $i = j$, the behaviour

$$\bar{\mathcal{E}}_{i,i}(\alpha, \Omega) = e_0^{(i)}(\alpha)[1 + e_2^{(i)}(\alpha)\Omega^2/2 + \cdots] \tag{3.3}$$

near the symmetry half plane $\Omega = 0$ of the wedge determines the profile $\langle \epsilon(r) \rangle_{\text{particle}}$ far from the dumbbell or lens and yields [9]

$$a_1^{(i)} = \mathcal{D}^{x_\epsilon} e_0^{(i)}(\alpha)/B_\epsilon^{1/2} \tag{3.4}$$

and

$$b_1^{(i)} = a_1^{(i)} \frac{\mathcal{D}^2}{8x_\epsilon(x_\epsilon + 1)} \left(e_2^{(i)}(\alpha) - x_\epsilon\right) \tag{3.5}$$

for two leading coefficients in the small particle expansion.

The boundary-induced density profile $\langle T_{\kappa\lambda}(\hat{r}) \rangle_{\text{wedge}}$ of the stress tensor in the wedge is given by

$$\langle T_{\kappa\lambda}(\hat{r}_e, \rho, \Omega) \rangle_{\text{wedge}}^{(i,j)} = \rho^{-d} \tau_{i,j}(\alpha)[\delta_{\kappa\lambda} - d u_\kappa^{(n)}(\Omega) u_\lambda^{(n)}(\Omega)], \tag{3.6}$$

where $u^{(n)}(\Omega)$ is the unit vector normal to the half plane $\Omega = \text{const}$ which contains $\hat{r}$, as in the left-hand side of figure 2. Unlike (3.1) there is no non-universal amplitude in (3.6), and the ρ-exponent and the Ω-dependence are trivial. Only the variation of the universal amplitude τ with the opening angle α of the wedge depends on the bulk universality class and the surface classes i, j, and remains to be determined. The stress tensor density (3.6) has a vanishing trace and obeys the continuity equation, as discussed in appendix A.

We note two special cases. (i) For $\alpha \to \pi$ and $i = j$ the wedge becomes the half space with a uniform boundary, and $\tau \to 0$ since the stress tensor density vanishes [10]. According to the left-hand side of figure 2, only for $\tau = 0$ is (3.6) consistent with the symmetries of the half space. (ii) For $\alpha \to 0$, τ diverges as

$$\tau_{i,j} \to \alpha^{-d}(-\Delta_{i,j}), \tag{3.7}$$

where $\Delta_{i,j}$ is the universal amplitude which determines the stress tensor density in the parallel plate geometry [10]. If the width of the film is ω and both tensor components are parallel to the plates, $\langle T_{\text{parallel,parallel}}\rangle^{(i,j)}_{\text{film}} = \omega^{-d}(-\Delta_{i,j})$.

Using the inversion transformation for the conformal stress tensor [13, 9] one finds from equation (3.6) the stress tensor density

$$\langle T_{kl}(\boldsymbol{r})\rangle^{(i,j)}_{\text{particle}} = (\mathcal{D}/\Lambda^2)^d \tau_{i,j}(\alpha)[\delta_{kl} - d u_k^{(N)}(\boldsymbol{r}) u_l^{(N)}(\boldsymbol{r})] \tag{3.8}$$

outside the dumbbell or lens. Here

$$\Lambda^2 = \sqrt{[r^2 - (\mathcal{D}/2)^2]^2 + \mathcal{D}^2 r_\parallel^2} \tag{3.9}$$

with r and $r_\parallel$ the distance of point $\boldsymbol{r}$ from the particle centre and its component parallel to the particle rotation axis. The inverse length $\mathcal{D}/\Lambda^2$ in (3.8) equals $b(\hat{\boldsymbol{r}})/\rho(\hat{\boldsymbol{r}})$, where b is the dilatation factor $|\det(\partial\hat{\boldsymbol{r}}/\partial\boldsymbol{r})|^{1/d}$ of the conformal mapping, and diverges as $(r_\parallel, r) \to (0, \mathcal{D}/2)$, as the circle C of intersection is approached. The unit vector $\boldsymbol{u}^{(N)}$ in the particle geometry is the counterpart of $\boldsymbol{u}^{(n)}$ in the wedge geometry. It points along the surface normal at $\boldsymbol{r}$ of the spherical surface portion $S_{C,\boldsymbol{r}}$ which contains $\boldsymbol{r}$ and is bounded by the circle C. $S_{C,\boldsymbol{r}}$ is the image of the half plane $\Omega = \text{const}$ which contains $\hat{\boldsymbol{r}}$. With the particle axis $\parallel$ as one of the Cartesian directions,

$$u_k^{(N)}(\boldsymbol{r}) = \Lambda^{-2}\{\delta_{k\parallel}[r^2 - (\mathcal{D}/2)^2] - 2r_k r_\parallel\}. \tag{3.10}$$

The vector field $\boldsymbol{u}^{(N)}$ for given $\mathcal{D}$ is shown on the right-hand side of figure 2. Both $\boldsymbol{u}^{(N)}$ and $\boldsymbol{u}^{(n)}$ are *independent* of α and the bulk and surface universality classes i, j.

In leading order $\mathcal{D} \ll r$,

$$\langle T_{kl}(\boldsymbol{r})\rangle^{(i,j)}_{\text{particle}} \to (\mathcal{D}/r^2)^d \tau_{i,j}(\alpha)[\delta_{kl} - d\mathcal{I}_{k,\parallel}\mathcal{I}_{l,\parallel}], \tag{3.11}$$

with

$$\mathcal{I}_{k,m} \equiv \mathcal{I}_{k,m}(\boldsymbol{r}) = \delta_{k,m} - 2r_k r_m/r^2. \tag{3.12}$$

On comparing with the stress tensor correlation function

$$\langle T_{kl}(\boldsymbol{r})T_{mn}(0)\rangle_{\text{bulk}} = B_T r^{-2d}\{(1/2)[\mathcal{I}_{k,m}\mathcal{I}_{l,n} + \mathcal{I}_{k,n}\mathcal{I}_{l,m}] - (1/d)\delta_{kl}\delta_{mn}\} \tag{3.13}$$

in unbounded bulk [13, 14, 9], equation (3.11) implies that

$$\langle T_{kl}(\boldsymbol{r})\rangle^{(i,j)}_{\text{particle}} \to b_2^{(i,j)}\langle T_{kl}(\boldsymbol{r})T_{\parallel\parallel}(0)\rangle_{\text{bulk}}, \qquad \mathcal{D} \ll r, \tag{3.14}$$

with the stress tensor contribution in the small particle expansion given by

$$b_2^{(i,j)}T_{\parallel\parallel} = -\mathcal{D}^d \tau_{i,j}(\alpha)\frac{d}{B_T}T_{\parallel\parallel}. \tag{3.15}$$

For the special case $\alpha \to 0$, where $\mathcal{D} \to \alpha L/2$ and equation (3.7) applies, equation (3.15) reduces to the expression $b_2^{(i,j)} \to (L/2)^d \Delta_{i,j} d/B_T$ for a dumbbell of two touching spheres with diameter L, given in equation (2.15) of [9].

The form of $\langle T\rangle^{(i,j)}_{\text{wedge}}$ in (3.6) has been calculated for special cases. See [10, 15] for $d = 2$, [12] for symmetry breaking surfaces $i = j$ as $d \to 4$, and appendix B for Dirichlet boundaries and $\alpha = \pi/2$. Here we indicate how (3.6) can be derived in the general case. For $\boldsymbol{r}$ on the particle rotation axis, $\langle T\rangle^{(i,j)}_{\text{particle}}$ must have an eigenvector parallel to the axis, by rotation symmetry. That the particle axis is the image of a circle in the plane $\hat{\boldsymbol{r}}_e = 0$ of the wedge with centre in the edge and passing through the centre of inversion, see the long dashes in figures 1 and 2, implies an eigenvector $\boldsymbol{u}^{(n)}$ of $\langle T\rangle^{(i,j)}_{\text{wedge}}$ tangent to this circle. Likewise, degenerate eigenvectors perpendicular to the axis imply $d - 1$ degenerate eigenvectors perpendicular to $\boldsymbol{u}^{(n)}$. The simple form (3.6) of the symmetric, traceless, and conformal tensor density $\langle T\rangle$

for the wedge then follows from scaling (dilatation symmetry), translation, and reflection symmetry in the edge-subspace, and the Ω-independence of τ is due to the continuity equation of the stress tensor; see appendix A. In appendix B we also discuss, within the Gaussian model, the more complicated form of the density $\langle T^{(\mathrm{can})}\rangle_{\mathrm{wedge}}$ of the *canonical* stress tensor, which also obeys the continuity equation, but is not trace-free and not a conformal tensor, and for which $\boldsymbol{u}^{(n)}(\Omega)$, in general, is not an eigenvector. Its eigenvalues depend on both ρ and Ω, and some of the eigenvalues diverge as the boundary planes of the wedge are approached. The simple form (3.6) is recovered on adding the 'improvement-term' [16].

We briefly comment on particle shapes where the *horizontal* axis on the right-hand side of figure 1 (passing through the small triangle and square) is the rotation axis. These particles resemble an apple (self-intersecting torus) for $\alpha < \pi$ and an American football for $\alpha > \pi$, and could be conformally mapped onto a *cone* with opening angle α.

4. Gaussian model with Dirichlet boundaries

In $d = 2$ spatial dimensions, a wedge can be obtained from the half plane by means of an appropriate conformal transformation. The dependence on the angle α only enters via the transformation and is to a large extent model independent. For example, for $i = j$, the stress amplitude τ is independent of the surface universality class i and equals $[(\pi/\alpha)^2 - 1]c/(24\pi)$, where only the universal bulk constant c, the 'conformal charge', depends on the model class. Using (3.7), this is consistent with the i-independent film amplitude $\Delta_{i,i} = -\pi c/24$ for a strip with equal boundary conditions [10]. Also the form of the scaling functions $\bar{\mathcal{P}}_{i,i} = \mathcal{A}_{\mathcal{O}}^{(i)}[(\alpha/\pi)\cos(\pi\Omega/\alpha)]^{-x_{\mathcal{O}}}$ is to a large extent model independent [11] and is completely determined by the bulk scaling index $x_{\mathcal{O}}$ and the universal, but i-dependent, half-space boundary amplitude $\mathcal{A}_{\mathcal{O}}^{(i)}$ of the scalar operator $\mathcal{O}$. For i not equal to j, the stress amplitude $\tau_{i,j} = -(c/(24\pi)) - \Delta_{i,j}/\alpha^2$ also depends on the boundary universality classes. Since $\Delta_{i,j}$ for $i \neq j$ is in general different from $-\pi c/24$, $\tau_{i,j}$ is non-vanishing even for $\alpha = \pi$, i.e. for the half plane with a non-homogeneous boundary [15].

In $d > 2$, however, no such conformal transformation exists, and the α-dependent quantities $\bar{\mathcal{P}}$ and τ depend on the bulk and surface universality classes in a much stronger way. In particular a bulk amplitude (like c) and the parallel plate amplitude, $\Delta_{i,j}$, are not sufficient to predict $\tau_{i,j}(\alpha)$.

For the Gaussian Ginzburg–Landau field theory (2.1) at the critical point $t = 0$ in $d > 2$ spatial dimensions, the scaling function $\bar{\mathcal{E}}$ of the energy density in the wedge is given by

$$\bar{\mathcal{E}} = -\langle\Phi^2(\hat{\boldsymbol{r}})\rangle_{\mathrm{wedge}}\rho^{d-2}/(\sqrt{2}\tilde{S}_d), \qquad \tilde{S}_d = \pi^{-d/2}\Gamma((d/2)-1)/4, \quad (4.1)$$

where we have suppressed the indices $(i, j) = (\mathrm{D}, \mathrm{D})$ with D for Dirichlet (see footnote 3). The stress tensor in the Gaussian model is the sum [16]

$$T_{\kappa\lambda}(\hat{\boldsymbol{r}}) = T_{\kappa\lambda}^{(\mathrm{can})}(\hat{\boldsymbol{r}}) - I_{\kappa\lambda}(\hat{\boldsymbol{r}}) \qquad (4.2)$$

of the canonical stress tensor

$$T_{\kappa\lambda}^{(\mathrm{can})}(\hat{\boldsymbol{r}}) = (\hat{\partial}_\kappa\Phi(\hat{\boldsymbol{r}}))(\hat{\partial}_\lambda\Phi(\hat{\boldsymbol{r}})) - \delta_{\kappa\lambda}(\hat{\nabla}\Phi(\hat{\boldsymbol{r}}))^2/2 \qquad (4.3)$$

and the so-called improvement term with

$$I_{\kappa\lambda}(\hat{\boldsymbol{r}}) = \frac{1}{4}\frac{d-2}{d-1}[\hat{\partial}_\kappa\hat{\partial}_\lambda - \delta_{\kappa\lambda}\hat{\Delta}]\Phi^2(\hat{\boldsymbol{r}}). \qquad (4.4)$$

Unlike $T^{(\mathrm{can})}$, the density of T in (4.2) has a vanishing trace and transforms as a conformal tensor; see appendices B and C. The bulk amplitude B_T in (3.13) equals $[\tilde{S}_d(d-2)]^2 d/(d-1)$ for the Gaussian model.

The boundary-induced densities $\langle\Phi^2(\hat{r})\rangle_{\text{wedge}}$ and $\langle T_{\kappa\lambda}(\hat{r})\rangle_{\text{wedge}}$ follow in an obvious way from the boundary-induced contribution $\delta\langle\hat{\varphi}_{12}\rangle_{\text{wedge}}$ of the propagator in the wedge

$$\langle\hat{\varphi}_{12}\rangle_{\text{wedge}} = \langle\hat{\varphi}_{12}\rangle_{\text{bulk}} + \delta\langle\hat{\varphi}_{12}\rangle_{\text{wedge}}, \tag{4.5}$$

with

$$\hat{\varphi}_{12} = \Phi(\hat{r}_1)\Phi(\hat{r}_2). \tag{4.6}$$

For the special opening angles $\alpha = \pi/g$, with g a positive integer, $\delta\langle\hat{\varphi}_{12}\rangle_{\text{wedge}}$ is a linear combination of $2g - 1$ bulk propagators from r_1 to images of r_2; see appendix B.

In order to determine e_0, e_2 in (3.3) and τ in (3.6) for *arbitrary* α, we use the representation of [17] at the critical point

$$\langle\hat{\varphi}_{12}\rangle_{\text{wedge}} = \int d^{d-2}q\,(2\pi)^{2-d}e^{iq(\hat{r}_{e1}-\hat{r}_{e2})}(2/\alpha)\sum_{m=1}^{\infty} I_{m\pi/\alpha}(q\rho_<)K_{m\pi/\alpha}(q\rho_>)$$
$$\times \sin\left[m\pi\left(\frac{1}{2}+\frac{\Omega_1}{\alpha}\right)\right]\sin\left[m\pi\left(\frac{1}{2}+\frac{\Omega_2}{\alpha}\right)\right], \tag{4.7}$$

where $\rho_< = \min(\rho_1, \rho_2)$, $\rho_> = \max(\rho_1, \rho_2)$, and I and K are modified Bessel functions. A more explicit expression arises for $(\hat{r}_{e1}, \rho_1) = (\hat{r}_{e2}, \rho_2)$. Using

$$\int_0^\infty dx\,x^{2A-1}I_{m\pi/\alpha}(x)K_{m\pi/\alpha}(x) = 2^{2A-2}\frac{\Gamma(A)}{\Gamma(1-A)}\int_0^1 dt\,t^{m\pi/\alpha}t^{A-1}(1-t)^{-2A} \tag{4.8}$$

for $2A = d - 2$ in order to rewrite the q-integral in a form where the m-summation can be done [17], one finds

$$\tilde{S}_d^{-1}\langle\hat{\varphi}_{12}\rangle_{\text{wedge}}|_{(\hat{r}_{e1},\rho_1)=(\hat{r}_{e2},\rho_2)} = -(2/\alpha)\sin(\pi d/2)\rho^{2-d}\int_0^1 dt\,\Psi_d(t)$$
$$\times\left\{\frac{1-t^{\pi/\alpha}\cos[(\Omega_1-\Omega_2)\pi/\alpha]}{1+t^{2\pi/\alpha}-2t^{\pi/\alpha}\cos[(\Omega_1-\Omega_2)\pi/\alpha]}\right.$$
$$\left.-\frac{1+t^{\pi/\alpha}\cos[(\Omega_1+\Omega_2)\pi/\alpha]}{1+t^{2\pi/\alpha}+2t^{\pi/\alpha}\cos[(\Omega_1+\Omega_2)\pi/\alpha]}\right\}, \tag{4.9}$$

where $\rho \equiv \rho_1 = \rho_2$ and

$$\Psi_d(t) = t^{(d-4)/2}(1-t)^{2-d}. \tag{4.10}$$

The expression in equation (4.9) satisfies the Dirichlet boundary conditions since the curly bracket vanishes for Ω_1 (or Ω_2) equal to $\alpha/2$ or $-\alpha/2$. For $\Omega_1 \neq \Omega_2$ the t-integral converges in the interval $2 - (2\pi/\alpha) < d < 4$ of spatial dimensions d with the lower and upper limits coming from the behaviours of the integrand for $t \searrow 0$ and $t \nearrow 1$, respectively. The bulk divergence $(\rho|\Omega_1 - \Omega_2|)^{2-d}$ for $|\Omega_1 - \Omega_2| \to 0$ and $d > 2$ contained in (4.9) comes from integrating the first term in curly brackets over a region near $t = 1$ where $1 - t$ is of the order of $|\Omega_1 - \Omega_2|$.

A convenient way to evaluate the boundary-induced density

$$\langle\Phi^2(\hat{r})\rangle_{\text{wedge}} = \lim_{\hat{r}_1\to\hat{r},\hat{r}_2\to\hat{r}} \delta\langle\hat{\varphi}_{12}\rangle_{\text{wedge}} \tag{4.11}$$

and its scaling function $\bar{\mathcal{E}}(\alpha, \Omega)$ in (4.1) for $d = 3$ by means of equation (4.9) is based on the observation that $\bar{\mathcal{E}}$ is an *analytic* function of d in an interval that includes both $d = 2$ and $d = 3$ as interior points. Since the limit $\hat{r}_1 \to \hat{r}, \hat{r}_2 \to \hat{r}$ of the bulk propagator

$\propto |\hat{r}_1 - \hat{r}_2|^{2-d}$ *vanishes* for $d < 2$ (while it is infinite for $d > 2$), one may replace $\delta\langle\hat{\varphi}_{12}\rangle_{\text{wedge}}$ by $\langle\hat{\varphi}_{12}\rangle_{\text{wedge}}$ and use (4.9), in calculating the limit in (4.11) for $d < 2$. This leads to

$$\bar{\mathcal{E}}(\alpha, \Omega) = (\sqrt{2}/\alpha) \sin(\pi d/2) \int_0^1 dt \, \Psi_d(t)$$

$$\times \left\{ \frac{1}{1 - t^{\pi/\alpha}} - \frac{1 + t^{\pi/\alpha} \cos(2\pi\Omega/\alpha)}{1 + t^{2\pi/\alpha} + 2t^{\pi/\alpha} \cos(2\pi\Omega/\alpha)} \right\}; \qquad d < 2, \qquad (4.12)$$

in terms of an integral which is well defined for $2 - (2\pi/\alpha) < d < 2$ and which has to be analytically continued[4] in order to obtain $\bar{\mathcal{E}}$ for $d = 3$.

For $e_0(\alpha) = \bar{\mathcal{E}}(\alpha, \Omega = 0)$ the integral in (4.12) becomes

$$J(\alpha, d) = \int_0^1 dt \, \Psi_d(t) t^{\pi/\alpha} \frac{2}{1 - t^{2\pi/\alpha}}, \qquad (4.13)$$

and the continuation can be made by rewriting J as the sum of $J^{(1)}$ and $J^{(2)}$, where

$$J^{(1)}(\alpha, d) = \int_0^1 dt \, \Psi_d(t) t^{\pi/\alpha} \left[\frac{2}{1 - t^{2\pi/\alpha}} - l(t) \right], \qquad (4.14)$$

and

$$J^{(2)}(\alpha, d) = \int_0^1 dt \, \Psi_d(t) t^{\pi/\alpha} l(t). \qquad (4.15)$$

Here

$$l(t) = \frac{\alpha/\pi}{1 - t} + 1 - \frac{\alpha}{2\pi} \qquad (4.16)$$

are the first two terms in the Laurent series of $2/(1 - t^{2\pi/\alpha})$ around $t = 1$ so that the integrability domain $2 - (2\pi/\alpha) < d < 4$ of $J^{(1)}$ extends up to $d = 4$. As a sum of beta-functions the continuation to $d = 3$ of the integral $J^{(2)}$ is trivial and yields $J^{(2)}(\alpha, 3) = -1$, implying

$$e_0(\alpha) = (\sqrt{2}/\alpha)[1 - J^{(1)}(\alpha, 3)], \qquad d = 3. \qquad (4.17)$$

Here $J^{(1)}(\alpha, 3)$ follows from the right-hand side in equation (4.14) on replacing Ψ_d by $\Psi_3 = t^{-1/2}/(1 - t)$, and for α arbitrary between 0 and 2π we have calculated it numerically. Using equation (3.4), the corresponding results for $a_1 B_\epsilon^{1/2}/L = \sin(\alpha/2)e_0(\alpha)$ in the interval $0 < \alpha < \pi$ and $a_1 B_\epsilon^{1/2}/\mathcal{D} = e_0(\alpha)$ in the interval $\pi < \alpha < 2\pi$ are shown in figure 3. Analytical results for some special values of α are given in table 1.

In the Gaussian model some amplitudes of isotropic operators beyond leading order in (2.5), such as Φ^4 and Φ^6, are also determined by a_1. The contributions $3\beta_I^2\Phi^4/4!$ and $-15\beta_I^3\Phi^6/6!$ of the non-leading isotropic operators Φ^4 and Φ^6 to σ_I on the right-hand side of equation (2.5) follow from the relations $\langle\Phi^4\rangle_{\text{particle}} = 3\langle\Phi^2\rangle_{\text{particle}}^2$ and $\langle\Phi^6\rangle_{\text{particle}} = 15\langle\Phi^2\rangle_{\text{particle}}^3$ between profiles due to Wick's theorem. Here β_I equals $a_1\sqrt{B_\epsilon}\sqrt{2}/\tilde{S}_d$ and appears in the leading isotropic contribution $a_1\epsilon = -\beta_I\Phi^2/2$ in the notation of [5]. For the sphere with $\alpha = \pi$ and $\beta_I = (L/2)^{d-2}/\tilde{S}_d$ and the dumbbell of two touching spheres with $\alpha = 0$ and $\beta_I = (L/2)^{d-2}2(1 - 2^{3-d})\zeta(d - 2)/\tilde{S}_d$ the role of these non-leading operators has been discussed in [4] and [9], respectively.

---

[4] For $\alpha = \pi/g$, where $\delta\langle\hat{\varphi}_{12}\rangle_{\text{wedge}}$ is a superposition of images, $\bar{\mathcal{E}}$ is an entire function of d. For example, $\bar{\mathcal{E}}$ is given by $(2\cos\Omega)^{2-d}/\sqrt{2}$ if $\alpha = \pi$, and by (B.5) if $\alpha = \pi/2$. For α arbitrary, the analytic continuation of $(\sqrt{2}/\alpha)\sin(\pi d/2)J^{(2)}$ with $J^{(2)}$ from (4.15), and thus of e_0, is an analytic function of d in the interval $2 - (2\pi/\alpha) < d < 4$. The continuation of e_0, after taking the limit in (4.11) below $d = 2$, coincides with the result from taking the limit above $d = 2$ directly, since both certainly coincide for $\alpha = \pi/g$ and are analytic in α. Similar statements apply to J_e in (D.7). Here the continuation of $J_e/\tilde{S}_d$ is an analytic function of d for $-(2\pi/\alpha) < d < 4$.
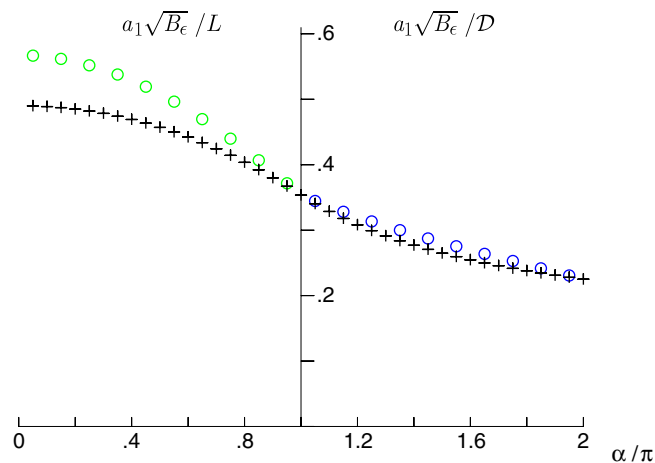
Figure 3. The leading amplitude a_1 in (2.5) for particles with Dirichlet boundary conditions in the Gaussian model. Crosses denote results for dumbbells ($0 < \alpha/\pi < 1$) and lenses ($1 < \alpha/\pi < 2$). Circles denote results for circumscribing prolate and oblate ellipsoids; see the paragraph containing equations (4.19) and (4.20). The oblate ellipsoid and the lens coincide for $\alpha/\pi = 1$ and 2, where they become a sphere and a disc, respectively.

Table 1. Amplitudes for dumbbells with $\alpha = 0$, $\pi/2$, the sphere ($\alpha = \pi$), and the disc ($\alpha = 2\pi$) in three spatial dimensions. Numbers in brackets denote amplitudes for prolate ellipsoids circumscribing the dumbbells. The values correspond to the crosses and circles in figures 3–5.

| α	0	$\pi/2$	π	2π	α
$a_1\sqrt{B_\epsilon}/L$	$2^{-1/2}\ln 2$ $= 0.490$ (0.569)	$2^{-1/2} - 2^{-2}$ $= 0.457$ (0.508)	$2^{-3/2}$ $= 0.354$	$2^{-1/2}\pi^{-1}$ $= 0.225$	$a_1\sqrt{B_\epsilon}/\mathcal{D}$
$b_1\sqrt{B_\epsilon}/L^3$	$7\zeta(3)/(64\sqrt{2})$ $= 0.0930$ (0.0561)	$(4+2^{-1/2})/(64\sqrt{2})$ $= 0.0520$ (0.0304)	0	$-5/(96\pi\sqrt{2})$ $= -0.0117$	$b_1\sqrt{B_\epsilon}/\mathcal{D}^3$
b_2/L^3	$-\pi\zeta(3)/4$ $= -0.944$ (-0.630)	$-\pi 2^{-5/2}$ $= -0.555$ (-0.346)	0	$1/6$ $= 0.166$	$b_2/\mathcal{D}^3$

To calculate the small particle anisotropy amplitude b_1 in (3.5), we need the coefficient $\propto \Omega^2$ of $\bar{\mathcal{E}}$. The contribution of order Ω^2 to the curly bracket in (4.12) contains a factor $1 - t^{\pi/\alpha}$ and leads to a convergent integral up to $d = 4$. Thus, no continuation is necessary, and

$$e_0(\alpha)e_2(\alpha) = (4\sqrt{2}\pi^2/\alpha^3)\int_0^1 dt\,\Psi_3(t)t^{\pi/\alpha}(1 - t^{\pi/\alpha})/(1 + t^{\pi/\alpha})^3, \qquad d = 3, \qquad (4.18)$$

which on using (3.5) with (3.4), (4.17) leads to the results for b_1 shown in figure 4 and in table 1.

In appendix D we use similar continuations in d to calculate the stress tensor amplitude $\tau(\alpha)$ from (3.6) and (4.2)–(4.4) in $d = 3$ with the result (D.15). The second anisotropy amplitude b_2 then follows from (3.15) and the value $d/B_T = 32\pi^2$, with the results shown in figure 5 and table 1.

It is interesting to compare dumbbells and lenses with ellipsoids. We compare a dumbbell with α between 0 and π with a prolate ellipsoid that circumscribes the dumbbell, touches it at the highest and lowest points, and has the same curvature at these points. Denoting by $D_\parallel$ and
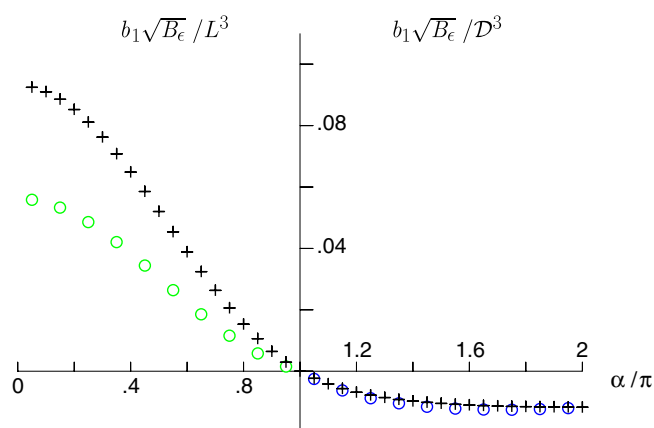
Figure 4. The anisotropy amplitude b_1 in (2.6).
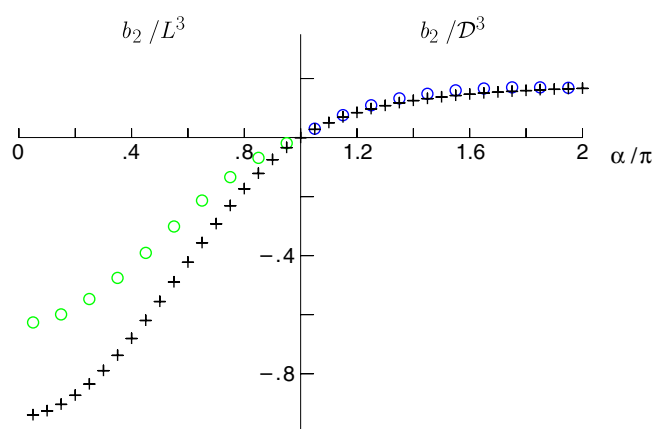
Figure 5. The anisotropy amplitude b_2 in (2.6).

$D_\perp$ the diameters of the ellipsoid parallel and perpendicular to the rotation axis,

$$D_\parallel = 2L \cos^2(\alpha/4), \qquad D_\perp = \sqrt{2}L \cos(\alpha/4). \tag{4.19}$$

Similarly, we compare a lens with α between π and 2π with an oblate circumscribing ellipsoid, so that

$$D_\parallel = \mathcal{D}\,\mathrm{ctg}(\alpha/4), \qquad D_\perp = \mathcal{D} \tag{4.20}$$

where $\mathcal{D}\,\mathrm{ctg}(\alpha/4)$ is the width [9] of the lens. The amplitudes a_1, b_1, b_2 of the ellipsoids are shown as circles in figures 3–5. They follow[5] from the expressions in footnote 2 and equations (180)–(185) in [5], where the long axis $[D_\parallel, D_\perp]$ and short axis $[D_\perp, D_\parallel]$ of the [prolate, oblate] ellipsoid is denoted by l and s, respectively.

As expected, the isotropic and anisotropic perturbations of the polymer system from dumbbells are weaker and stronger, respectively, than from the circumscribing prolate ellipsoids. The oblate ellipsoids have stronger isotropic perturbation amplitudes a_1 and also slightly stronger anisotropic amplitudes b_1 and b_2 than the lens.

---

[5] For the circumscribing ellipsoids in equations (4.19) and (4.20), the parameters $[f, \xi_E]$ of [5] are given by $[2^{-1/2}L \cos(\alpha/4)\sqrt{\cos(\alpha/2)}, 2^{1/2}/\sqrt{1 - \mathrm{tg}^2(\alpha/4)}]$ and $[(\mathcal{D}/2)\sqrt{1 - \mathrm{ctg}^2(\alpha/4)}, 1/\sqrt{\mathrm{tg}^2(\alpha/4) - 1}]$, respectively.

5. Weak anisotropy

Consider the amplitudes a_1, b_1, and b_2 for particles with a surface S' which deviates only slightly from the surface S of a sphere with radius R. S' is obtained by shifting each surface point r_S of S by a small amount $\eta(\theta_S)$ towards the centre of S at the origin. Here θ_S is the angle which r_S encloses with the particle rotation axis, and we consider particles with a centre of reflection so that $\eta(\theta_S) = \eta(\pi - \theta_S)$. For a dumbbell or lens with $\alpha = \pi + \delta\alpha$, we choose $R = L/2$ and obtain

$$\eta = \delta\alpha(L/4)|\cos\theta_S| \tag{5.1}$$

to first order in $\delta\alpha$. As expected from figure 1, η in (5.1) is non-analytic at $\theta_S = \pi/2$. At the end of section 3 we have introduced apple-and football-shaped particles with $\alpha = \pi + \delta\alpha$ smaller and larger than π, respectively. Nearly spherical particles of this family are generated by

$$\eta = \delta\alpha(L/4)\sin\theta_S. \tag{5.2}$$

For weakly anisotropic prolate and oblate ellipsoids with $D_\parallel > D_\perp$ and $D_\parallel < D_\perp$, respectively,

$$\eta = \frac{D_\parallel - D_\perp}{2}\sin^2\theta_S, \tag{5.3}$$

if we choose $R = D_\parallel/2$.

In the presence of the weakly anisotropic particle the propagator is given by [5]

$$\langle\varphi_{12}\rangle = \langle\varphi_{12}\rangle_{\text{sphere}} + \int dS\,\eta(\theta_S)\langle T_{\perp\perp}(r_S)\varphi_{12}\rangle_{\text{sphere}} \tag{5.4}$$

to first order in η. Here $\int dS$ is an integral over the surface S of the sphere, and $T_{\perp\perp}$ is the diagonal component of the stress tensor perpendicular to S. Due to the Dirichlet boundary condition and the form (4.2)–(4.4) of the stress tensor, $T_{\perp\perp}(r_S)$ can be replaced by $(\partial_\perp\Phi)^2/2$ in the correlation function in (5.4) with the result

$$\langle T_{\perp\perp}(r_S)\varphi_{12}\rangle_{\text{sphere}} = [(d-2)\tilde{S}_d]^2\frac{(r_1^2 - R^2)(r_2^2 - R^2)}{R^2(|r_1 - r_S||r_2 - r_S|)^d}, \tag{5.5}$$

and, from the behaviour of (5.4) for $R \ll r_1, r_2$, one finds[6]

$$a_1\sqrt{B_\epsilon} - R^{d-2}/\sqrt{2} = -\frac{(d-2)\Gamma(d/2)}{\sqrt{2\pi}\,\Gamma((d-1)/2)}R^{d-3}\int_0^\pi d\theta_S(\sin\theta_S)^{d-2}\eta(\theta_S), \tag{5.6}$$

$$b_1\sqrt{B_\epsilon}/b_2 = -\frac{1}{4\sqrt{2}\pi^{d/2}}\frac{d+1}{d-1}\Gamma((d+2)/2), \tag{5.7}$$

and

$$b_2 = R^{d-1}\frac{2\pi^{(d-1)/2}}{\Gamma((d+1)/2)}\int_0^\pi d\theta_S\,(\sin\theta_S)^{d-2}[d(\cos\theta_S)^2 - 1]\eta(\theta_S). \tag{5.8}$$

Explicit expressions for dumbbells or lenses, apples or footballs, and ellipsoids in an arbitrary spatial dimension d follow on inserting η from (5.1) to (5.3). In $d = 3$,

$$a_1\sqrt{B_\epsilon}/L = \frac{1}{2\sqrt{2}} - \delta\alpha\left(\frac{1}{8\sqrt{2}}, \frac{\pi}{16\sqrt{2}}\right),$$
$$b_2/L^3 = \delta\alpha\left(\frac{\pi}{16}, -\frac{\pi^2}{64}\right) \tag{5.9}$$

[6] For example from (5.4) one may calculate $\langle\Phi^2(r)\rangle$ and $\langle T_{kl}(r)\rangle$, and from the behaviour for $R \ll r$ obtain a_1, b_1, and b_2.

for (dumbbell or lens, apple or football), and

$$a_1\sqrt{B_\epsilon} = \frac{D_\parallel}{2\sqrt{2}} + \frac{D_\perp - D_\parallel}{3\sqrt{2}},$$

$$b_2 = (D_\perp - D_\parallel)D^2\frac{2\pi}{15} \tag{5.10}$$

for ellipsoids. In our first order calculation D may be either $D_\parallel$ or $D_\perp$. Note that b_2 is negative for the *prolate* shapes (dumbbell with $\delta\alpha < 0$, football with $\delta\alpha > 0$, and prolate ellipsoid with $D_\parallel > D_\perp$) and positive for the *oblate* shapes (lens with $\delta\alpha > 0$, apple with $\delta\alpha < 0$, and oblate ellipsoid with $D_\parallel < D_\perp$).

The amplitudes b_1 follow from the amplitudes b_2 above via the ratio

$$b_1\sqrt{B_\epsilon}/b_2 = -\frac{3}{8\pi\sqrt{2}}. \tag{5.11}$$

For a nearly spherical particle with rotation axis and reflection symmetry, the ratio of the anisotropy amplitudes b_1 and b_2 is *independent* of its shape, see (5.7) and (5.11), but the ratio becomes shape dependent for larger deviations from spherical. For example,

$$b_1\sqrt{B_\epsilon}/b_2 = -\frac{1}{\pi}\left(\frac{7}{16\sqrt{2}}, \frac{8+\sqrt{2}}{32}, \frac{5}{16\sqrt{2}}, \frac{\ln(2D_\parallel/D_\perp)}{4\sqrt{2}}\right) \tag{5.12}$$

for a dumbbell of two touching spheres, a dumbbell with $\alpha = \pi/2$, a disc, and an ellipsoidal needle with $D_\parallel \gg D_\perp$. For the dumbbell-lens and ellipsoid families the modulus of the negative ratio $b_1\sqrt{B_\epsilon}/b_2$ is monotonically decreasing on increasing α from 0 to 2π and $D_\perp/D_\parallel$ from 0 to ∞, respectively, i.e. on changing from more prolate to more oblate shapes.

6. Induced interactions

The expressions (2.3) for the free energy cost F and (2.4) for the Boltzmann factor $\exp(-\delta\mathcal{H})$ of a small particle determine the polymer-induced orientation-dependent interactions. In particular, the leading anisotropic interactions between a *particle and a wall*,

$$F_{\text{aniso}}^{(p,w)} = p_0(\cos^2\vartheta_P)\{b_1\sqrt{B_\epsilon}4\pi\sqrt{2}\mathcal{M}_h''(y) - b_2[f_0(y) + (1/2)f_0(y/2)]\}, \tag{6.1}$$

with the second derivative

$$\mathcal{M}_h'' = 4[f_0(y) - (1/2)f_0(y/2)] \tag{6.2}$$

of the bulk-normalized polymer density in the half space [5] with respect to

$$y = z_P/\mathcal{R}_g, \qquad z_P = \text{particle–wall distance}, \tag{6.3}$$

and between *two particles* P, Q,

$$F_{\text{aniso}}^{(P,Q)} = -p_0(\cos^2\varphi_P + \cos^2\varphi_Q)\sqrt{2}a_1\sqrt{B_\epsilon}\beta_{\text{VII}}r_{PQ}^{-1}$$

$$\times \{12x^{-2}f_2(x/2) + 6x^{-1}f_1(x/2) + f_0(x/2)\}, \tag{6.4}$$

with

$$x = r_{PQ}/\mathcal{R}_g, \tag{6.5}$$

$$r_{PQ} = |r_P - r_Q| = \text{particle–particle distance} \tag{6.6}$$

and

$$\beta_{\text{VII}} = [16\sqrt{2}\pi b_1\sqrt{B_\epsilon} + b_2]/2, \tag{6.7}$$

follow from (2.3) with the half space perturbed by $\exp(-\delta\mathcal{H}) \propto \sigma_A(\mathrm{P})$ and the bulk perturbed by $\exp(-\delta\mathcal{H}) \propto \sigma_I(\mathrm{P})\sigma_A(\mathrm{Q}) + \sigma_I(\mathrm{Q})\sigma_A(\mathrm{P})$, respectively. Here $f_n = \mathrm{i}^n \mathrm{erfc}$ is the n-fold iterated complementary error function, ϑ_P is the angle between the particle axis and the surface normal of the boundary wall, and φ_P, φ_Q are the angles between the axes of particles P, Q and the distance vector $r_\mathrm{P} - r_\mathrm{Q}$ of the two particles. $F_{\mathrm{aniso}}^{(\mathrm{P},\mathrm{Q})}$ is proportional to the anisotropic part of $(\partial_{\|\mathrm{P}}^2 + \partial_{\|\mathrm{Q}}^2)K(r_{\mathrm{PQ}})$, with K the density–density correlation function of ideal polymers in bulk solution.

For a dumbbell or lens with any α the particle–wall expression predicts that, for small y, the particle orientation *parallel* to the wall and, for large y, the *perpendicular* orientation, have the lowest free energies. Note that $\mathcal{M}_\mathrm{h}$ has a point of inflection, and $\mathcal{M}_\mathrm{h}''$ is positive and negative for small and large y, respectively. With the values b_1 and b_2 from figures 4 and 5 above, the b_1 and b_2 contributions both favour the same, parallel orientation for small y. For large y they favour different orientations, and their sum is $\propto -\beta_{\mathrm{VII}}f_0(y/2)$, with β_{VII} from (6.7) in which b_1 dominates.

The two-particle expression predicts that particles align *parallel* to their distance vector, as expected from the attractive nature of the depletion interaction in a dilute polymer solution.

Qualitatively similar behaviour applies for prolate and oblate ellipsoids, where b_1 and b_2 can be taken from [4, 5] with the notation in footnote 2.

7. Summary and concluding remarks

We have studied the interaction between long flexible non-adsorbing polymers and mesoscopic colloidal dumbbells and lenses. The shape of the colloids is characterized by a parameter α, as shown in figure 1, and ranges from two touching spheres for $\alpha = 0$, to a sphere for $\alpha = \pi$, and to a disc for $\alpha = 2\pi$.

For small colloids and ideal polymers the amplitudes a_1, b_1, and b_2 in the small particle expansion (2.4), which determine the isotropic and anisotropic features of the interaction, are evaluated exactly for *arbitrary* α. They follow via the general relations (3.4), (3.5), and (3.15) from the results (4.17), (4.18), and (D.15) for density profiles of the Gaussian model in a wedge with opening angle α and Dirichlet boundary conditions, and are shown as crosses in figures 3–5. We compare with corresponding amplitudes for ellipsoids that circumscribe and touch the dumbbells and lenses; see equations (4.19), (4.20). Their values are shown as circles in figures 3–5. Analytical results for some special values of α are collected in table 1.

We also consider weakly anisotropic particles of general shapes with rotation axis and reflection centre; see equations (5.6)–(5.8). We find that the ratio b_1/b_2 in equations (5.7) and (5.11) of the two anisotropy amplitudes of these particles is *independent* of their shape. In particular we consider in equations (5.9) the shapes of a self-intersecting torus which resembles an apple and of an American football.

How to obtain from the amplitudes a_1, b_1, and b_2 the orientation-dependent polymer-induced interaction between particles is discussed in section 6. While the preferential alignment of two identical small particles is always parallel to their distance vector, see equation (6.4), the alignment of a particle with respect to a wall changes from perpendicular to parallel on decreasing the particle–wall distance; see equation (6.1). It would be interesting to check our predictions with simulations or real experiments.

The simple and general forms (3.6) and (3.8) of the density of the conformal stress tensor in a wedge and outside a dumbbell or lens, with eigenvectors shown in figure 2, follow from combining symmetries of the two geometries; see the end of section 3. We show in appendix C that the sum (4.2) of canonical tensor and improvement term is a conformal tensor, while

the separate terms are not and have densities with a more complicated form as discussed in appendix B.

Appendix A. Continuity equation in the wedge

Here we show that the Ω-independence of the prefactor $\tau_{i,j}$ in (3.6) follows from the continuity equation. For convenience we choose Cartesian axes perpendicular to the edge in the $\Omega = 0$ and $\Omega = \pi/2$ half planes and denote them by indices v and w, respectively, so that

$$(\hat{r}_v, \hat{r}_w) = \rho(\cos\Omega, \sin\Omega),$$
$$(u_v^{(n)}, u_w^{(n)}) = (-\sin\Omega, \cos\Omega), \tag{A.1}$$

and

$$\begin{pmatrix} \rho\partial\Omega/\partial\hat{r}_v, & \rho\partial\Omega/\partial\hat{r}_w \\ \partial\rho/\partial\hat{r}_v, & \partial\rho/\partial\hat{r}_w \end{pmatrix} = \begin{pmatrix} -\sin\Omega, & \cos\Omega \\ \cos\Omega, & \sin\Omega \end{pmatrix}. \tag{A.2}$$

Substituting (3.6) with $\tau_{i,j}(\alpha) \to \tau_{i,j}(\alpha, \Omega)$ into the two continuity equations [10]

$$\partial\langle T_{vv}\rangle_{\text{wedge}}/\partial\hat{r}_v + \partial\langle T_{vw}\rangle_{\text{wedge}}/\partial\hat{r}_w = 0$$
$$\partial\langle T_{wv}\rangle_{\text{wedge}}/\partial\hat{r}_v + \partial\langle T_{ww}\rangle_{\text{wedge}}/\partial\hat{r}_w = 0, \tag{A.3}$$

using (A.1), and calculating the derivatives by means of the chain rule and (A.2), one finds that the ρ-derivatives of the prefactor ρ^{-d} cancel the Ω-derivatives of the eigenvector $\boldsymbol{u}^{(n)}$. Only the Ω-derivatives of τ remain, and the left-hand sides of the first and second equation (A.3) are given by $(\partial\tau/\partial\Omega)(d-1)/\rho^{d+1}$ multiplied by $\sin\Omega$ and $-\cos\Omega$, respectively. Thus each of the two equations implies that τ is independent of Ω.

Appendix B. Wedge with $\alpha = \pi/2$

The propagator $\langle\hat{\varphi}_{12}\rangle_{\text{wedge}}$ for the Gaussian model in a wedge with Dirichlet boundary conditions and $\alpha = \pi/g$, with g an integer, can be obtained by the method of images. Besides the half space ($\alpha = \pi$) we consider here the simplest case of a wedge with $\alpha = \pi/2$ in which there are three images. With the notation

$$\hat{r}_{xi} = X_i, \qquad \hat{r}_{yi} = Y_i \tag{B.1}$$

for the components of

$$\hat{r}_i = (\hat{r}_{ei}, \hat{r}_{xi}, \hat{r}_{yi}); \qquad i = 1, 2 \tag{B.2}$$

perpendicular to the edge along Cartesian axes in the two boundary half planes $\Omega = -\pi/4$ (i.e. $Y = 0$, $X \geqslant 0$) and $\Omega = \pi/4$ (i.e. $X = 0$, $Y \geqslant 0$), the propagator at the critical point has the form (4.5) with

$$\langle\hat{\varphi}_{12}\rangle_{\text{bulk}} = \tilde{S}_d[\mathbf{e}_{12}^2 + (X_1 - X_2)^2 + (Y_1 - Y_2)^2]^{-(d-2)/2}, \tag{B.3}$$

and

$$\delta\langle\hat{\varphi}_{12}\rangle_{\text{wedge}} = \tilde{S}_d\{-[\mathbf{e}_{12}^2 + (X_1 + X_2)^2 + (Y_1 - Y_2)^2]^{-(d-2)/2}$$
$$+ [\mathbf{e}_{12}^2 + (X_1 + X_2)^2 + (Y_1 + Y_2)^2]^{-(d-2)/2}$$
$$- [\mathbf{e}_{12}^2 + (X_1 - X_2)^2 + (Y_1 + Y_2)^2]^{-(d-2)/2}\}. \tag{B.4}$$

Here $\mathbf{e}_{12}^2 \equiv (\hat{r}_{e1} - \hat{r}_{e2})^2$, and $\tilde{S}_d$ is defined in (4.1).

Letting $\hat{r}_1 \to \hat{r}$, $\hat{r}_2 \to \hat{r}$ on the right-hand side of (B.4) leads to the boundary-induced profile

$$-\bar{\mathcal{E}}(\rho/2)^{2-d}\sqrt{2} \equiv \langle \Phi^2(\hat{r}) \rangle_{\text{wedge}} 2^{d-2}/\tilde{S}_d = -X^{2-d} - Y^{2-d} + \rho^{2-d} \qquad \text{(B.5)}$$

of the energy density in (4.1), which due to

$$X \equiv \hat{r}_x = \rho(\cos\Omega - \sin\Omega)/\sqrt{2}, \qquad Y \equiv \hat{r}_y = \rho(\cos\Omega + \sin\Omega)/\sqrt{2} \qquad \text{(B.6)}$$

is in accordance with the general form (3.1) of a scalar density with bulk exponent $x_{\mathcal{O}} = d - 2$. It diverges on approaching the boundary planes $\Omega = \pm\pi/4$.

For the boundary-induced densities of the canonical stress tensor (4.3) and the 'improvement'-term (4.4),

$$\left(\langle T_{\kappa\lambda}^{(\text{can})}(\hat{r}) \rangle_{\text{wedge}}, \langle -I_{\kappa\lambda}(\hat{r}) \rangle_{\text{wedge}} \right) = (d-2)\tilde{S}_d 2^{-d}\left(\mathcal{T}_{\kappa\lambda}, -\mathcal{J}_{\kappa\lambda} \right), \qquad \text{(B.7)}$$

equation (B.4) yields

$$\begin{aligned}
\mathcal{T}_{xx} &= (d-2)Y^{-d} + d\rho^{-d-2}X^2 - (d-1)\rho^{-d} \\
\mathcal{T}_{xy} &= d\rho^{-d-2}XY \\
\mathcal{T}_{\text{e}\beta\text{e}\beta} &= (d-2)\left(X^{-d} + Y^{-d} \right) - (d-3)\rho^{-d}
\end{aligned} \qquad \text{(B.8)}$$

and

$$\begin{aligned}
-\mathcal{J}_{xx} &= -(d-2)Y^{-d} - [d(d-2)/(d-1)]\rho^{-d-2}X^2 + (d-2)\rho^{-d} \\
-\mathcal{J}_{xy} &= -[d(d-2)/(d-1)]\rho^{-d-2}XY \\
-\mathcal{J}_{\text{e}\beta\text{e}\beta} &= -(d-2)\left(X^{-d} + Y^{-d} \right) + [(d-2)^2/(d-1)]\rho^{-d}.
\end{aligned} \qquad \text{(B.9)}$$

Here $\text{e}\beta$ with $\beta = 3, \ldots, d$ runs over the $d-2$ Cartesian directions of the edge-subspace. $\mathcal{T}_{yy}$ and $-\mathcal{J}_{yy}$ follow from the above expressions for $\mathcal{T}_{xx}$ and $-\mathcal{J}_{xx}$ on exchanging X and Y. All other components of $\langle T^{(\text{can})} \rangle$ and $\langle -I \rangle$ vanish by symmetry.

In the sum $\mathcal{T}_{\kappa\lambda} - \mathcal{J}_{\kappa\lambda}$ all contributions proportional to X^{-d} and Y^{-d} cancel, and the density of the stress tensor T in (4.2) has the simple form of (3.6) with

$$\tau(\alpha = \pi/2) = 2^{-d}\frac{d-2}{d-1}\tilde{S}_d \qquad \text{(B.10)}$$

implying

$$b_2/L^d = -2(\pi/8)^{d/2}/\Gamma(d/2) \qquad \text{(B.11)}$$

if one uses (3.15) with $\mathcal{D}/L = 1/\sqrt{2}$ and the forms of B_T below (4.4) and $\tilde{S}_d$ in (4.1).

However, the densities of $T^{(\text{can})}$ and I separately have non-vanishing traces, with

$$\mathcal{T}_{xx} + \mathcal{T}_{yy} + \sum_{\beta=3}^{d} \mathcal{T}_{\text{e}\beta\text{e}\beta} = -\langle(\nabla\Phi)^2\rangle 2^{d-1}/\tilde{S}_d$$

$$= (d-2)[(d-1)(X^{-d} + Y^{-d}) - (d-2)\rho^{-d}], \qquad \text{(B.12)}$$

and a more complicated form. For example, their diagonal components parallel to the edge, and the trace (B.12), depend not only on ρ but, due to the terms $\propto X^{-d} + Y^{-d}$, also on Ω, and diverge on approaching the boundaries $X = 0$ or $Y = 0$. There is a corresponding divergence of the diagonal components of $T^{(\text{can})}$ and I parallel to a Dirichlet boundary wall for the half space ($\alpha = \pi$). Moreover, $u^{(n)}$ of equation (3.6) and figure 2 is, in general, not an eigenvector of $\langle T^{(\text{can})} \rangle$, due to the terms proportional to Y^{-d} and X^{-d} in $\mathcal{T}_{xx}$ and $\mathcal{T}_{yy}$, respectively. In the continuity equation satisfied by $\langle T^{(\text{can})} \rangle$, these terms do not contribute.

Appendix C. Conformal stress density

Here we verify that in the Gaussian model the boundary-induced profile $\langle T \rangle$, with T the sum (4.2) of the canonical stress tensor and the improvement term, is a conformal tensor. For a conformal transformation $\hat{r}' \to r'$ which leads from a geometry $\hat{G}'$ to a geometry G', we use the transformation law

$$\delta\langle \Phi(r_1')\Phi(r_2')\rangle_{G'} = (b(\hat{r}_1')b(\hat{r}_2'))^{(d-2)/2}\delta\langle \Phi(\hat{r}_1')\Phi(\hat{r}_2')\rangle_{\hat{G}'} \tag{C.1}$$

for the propagator $\delta\langle\Phi\Phi\rangle$ with bulk contribution subtracted as in (4.5). The dilatation factor $b(\hat{r}')$ of the transformation is defined below equation (3.9). Consider the boundary-induced density $\langle T_{kl}(r')\rangle_{G'}$, where T_{kl} follows from (4.2) on replacing $(\kappa, \lambda, \hat{r})$ by (k, l, r'). As in appendix B, each of its contributions follows from the subtracted propagator on the left-hand side of (C.1) by appropriate differentiations, where for the terms in $-\langle I_{kl}\rangle_{G'}$ and $\langle T_{kl}^{(\text{can})}\rangle_{G'}$ the arguments r_1' and r_2' are set equal to r' before and after differentiating, respectively. Following the same steps on the right-hand side of (C.1), one finds that in the sum $\langle T_{kl}\rangle_{G'} = \langle T_{kl}^{(\text{can})}\rangle_{G'} - \langle I_{kl}\rangle_{G'}$ the contributions involving r'-derivatives of b that come from calculating $T^{(\text{can})}$ *cancel* the contributions involving r'-derivatives of $\partial\hat{r}'/\partial r'$ and b that come from calculating $-I$ and one is left with the transformation formula

$$\langle T_{kl}(r')\rangle_{G'} = \sum_{\kappa,\lambda} b^{d-2}(\hat{r}')\left(\frac{\partial\hat{r}_\kappa'}{\partial r_k'}\right)\left(\frac{\partial\hat{r}_\lambda'}{\partial r_l'}\right)\langle T_{\kappa\lambda}(\hat{r}')\rangle_{\hat{G}'} \tag{C.2}$$

of a conformal tensor. In general $T^{(\text{can})}$ and I separately do not satisfy a transformation law of the form of (C.2). It is instructive to explicitly check the above arguments for the inversion $\hat{r}' = L^2 r'/r'^2$, where

$$\frac{\partial\hat{r}_\kappa'}{\partial r_k'} = b(\hat{r}')\mathcal{I}_{\kappa,k}(r'), \qquad b(\hat{r}') = \frac{L^2}{r'^2}, \tag{C.3}$$

with $\mathcal{I}$ defined in equation (3.12), and where (C.2) reduces to the transformation law of equations (2.36) and (2.37) in [9].

The transformation formula (C.2) for the stress tensor density is also expected to apply beyond the Gaussian model. Given in geometry $\hat{G}'$ an eigenvector of $\langle T(\hat{r}')\rangle_{\hat{G}'}$ which points along a certain distance vector $\mathrm{d}\hat{r}'$ and belongs to an eigenvalue $\hat{t}$, equation (C.2) implies in geometry G' an eigenvector of $\langle T(r')\rangle_{G'}$ which points along the corresponding distance vector $\mathrm{d}r'$ and belongs to the eigenvalue $b^d(\hat{r}')\hat{t}$.

Appendix D. Stress amplitude for arbitrary opening angle

It is convenient to calculate $\tau(\alpha)$ from (3.6) with $\kappa = \lambda$ equal to an edge direction $\mathrm{e}\beta$. Using (4.2)–(4.4) and the property

$$2\langle(\nabla\Phi)^2\rangle_{\text{wedge}} = \Delta\langle\Phi^2\rangle_{\text{wedge}} \tag{D.1}$$

of the vanishing trace of $\langle T^{(\text{can})} - I\rangle_{\text{wedge}}$, this yields

$$\tau(\alpha) = \rho^d\langle T_{\mathrm{e}\beta\mathrm{e}\beta}\rangle = \rho^d\left[\langle(\Phi_{\mathrm{e}\beta})^2\rangle_{\text{wedge}} - \frac{1}{4(d-1)}\Delta\langle\Phi^2\rangle_{\text{wedge}}\right], \tag{D.2}$$

where

$$\Phi_{\mathrm{e}\beta}(\hat{r}) = \partial\Phi(\hat{r})/\partial\hat{r}_{\mathrm{e}\beta}. \tag{D.3}$$

Since the boundary-induced profile

$$\langle(\Phi_{\mathrm{e}\beta}(\hat{r}))^2\rangle_{\text{wedge}} = \lim_{\hat{r}_1\to\hat{r},\hat{r}_2\to\hat{r}}[\langle\Phi_{\mathrm{e}\beta}(\hat{r}_1)\Phi_{\mathrm{e}\beta}(\hat{r}_2)\rangle_{\text{wedge}} - \langle\Phi_{\mathrm{e}\beta}(\hat{r}_1)\Phi_{\mathrm{e}\beta}(\hat{r}_2)\rangle_{\text{bulk}}] \tag{D.4}$$

is, apart from a factor $\tilde{S}_d$, analytic (see footnote 4) in d, the calculation proceeds similar to (4.11)–(4.17). We consider $d < 0$, where

$$\langle \Phi_{e\beta}(\hat{r}_1)\Phi_{e\beta}(\hat{r}_2)\rangle_{\text{bulk}} = (d-2)[|\hat{r}_1 - \hat{r}_2|^2 - d(\hat{r}_{1e\beta} - \hat{r}_{2e\beta})^2]|\hat{r}_1 - \hat{r}_2|^{-2-d}\tilde{S}_d \tag{D.5}$$

does not contribute on the right-hand side of (D.4), and find for $\Omega = 0$

$$\rho^d \langle (\Phi_{e\beta}(\hat{r}))^2\rangle_{\text{wedge}}|_{\Omega=0} = 2\pi^{(2-d)/2}\frac{1}{\alpha\Gamma(1-(d/2))}J_e, \tag{D.6}$$

with

$$J_e = \int_0^1 dt\, \Xi_d(t)t^{\pi/\alpha}\frac{1}{1 - t^{2\pi/\alpha}}, \tag{D.7}$$

where

$$\Xi_d(t) = t^{(d-2)/2}(1-t)^{-d}. \tag{D.8}$$

Here we have rewritten $\langle(\Phi_{e\beta})^2\rangle_{\text{wedge}}$ as $\sum_\beta \langle(\Phi_{e\beta})^2\rangle_{\text{wedge}}/(d-2)$ and used equations (4.7) and (4.8) with $2A = d$. The integral (D.7) converges for $-2\pi/\alpha < d < 0$.

Writing J_e as the sum of

$$J_e^{(1)} = \int_0^1 dt\, \Xi_d(t)t^{\pi/\alpha}\left[\frac{1}{1 - t^{2\pi/\alpha}} - k(t)\right] \tag{D.9}$$

and

$$J_e^{(2)} = \int_0^1 dt\, \Xi_d(t)t^{\pi/\alpha}k(t), \tag{D.10}$$

with

$$k(t) = \frac{\alpha}{2\pi}\frac{1}{1-t} + \frac{1}{2}\left(1 - \frac{\alpha}{2\pi}\right) + \frac{1}{24}\left(\frac{2\pi}{\alpha} - \frac{\alpha}{2\pi}\right)[2(1-t) + (1-t)^2], \tag{D.11}$$

the continuation to $d = 3$ leads to

$$J_e^{(2)}(\alpha, 3) = \frac{1}{72}\left[\left(\frac{2\pi}{\alpha}\right)^2 - 1 + 6\frac{\alpha}{2\pi}\right], \tag{D.12}$$

yielding

$$\langle(\Phi_{e\beta}(\hat{r}))^2\rangle_{\text{wedge}}|_{\Omega=0}\rho^d = -\frac{1}{\alpha\pi}[J_e^{(1)}(\alpha, 3) + J_e^{(2)}(\alpha, 3)] \tag{D.13}$$

in $d = 3$ where $J_e^{(1)}(\alpha, 3)$ follows from (D.9) on replacing Ξ_d by $\Xi_3 = t^{1/2}(1-t)^{-3}$.

In the second contribution to τ in (D.2),

$$\rho^d \Delta\langle\Phi^2\rangle_{\text{wedge}} = -\sqrt{2}\tilde{S}_d\{\partial_\Omega^2\bar{\mathcal{E}} + (d-2)^2\bar{\mathcal{E}}\} \tag{D.14}$$

can, for $\Omega = 0$ and $d = 3$, be expressed by e_0 and e_2 in (4.17), (4.18), so that

$$\tau(\alpha) = -\frac{1}{\alpha\pi}[J_e^{(1)}(\alpha, 3) + J_e^{(2)}(\alpha, 3)] + \frac{1}{16\sqrt{2}\pi}e_0(\alpha)[e_2(\alpha) + 1]. \tag{D.15}$$

References

[1] Rudhardt D, Bechinger C and Leiderer P 1998 *Phys. Rev. Lett.* **81** 1330
[2] van Blaaderen A 2003 *Science* **301** 470
    van Blaaderen A 2004 *Mater. Res. Soc. Bull.* (February) 85
[3] Snoeks E *et al* 2000 *Adv. Mater.* **12** 1511
[4] Eisenriegler E, Bringer A and Maaßen R 2003 *J. Chem. Phys.* **118** 8093
[5] Eisenriegler E 2005 *Soft Condensed Matter* ed G Gompper and M Schick (Weinheim: Wiley–VCH)
[6] de Gennes P G 1979 *Scaling Concepts in Polymer Physics* (Ithaca, NY: Cornell University Press)
[7] Burkhardt T W and Eisenriegler E 1995 *Phys. Rev. Lett.* **74** 3189
    Burkhardt T W and Eisenriegler E 1997 *Phys. Rev. Lett.* **78** 2867
[8] Eisenriegler E and Ritschel U 1995 *Phys. Rev.* B **51** 13717
[9] Eisenriegler E 2004 *J. Chem. Phys.* **121** 3299
[10] Cardy J L 1986 *Phase Transitions and Critical Phenomena* vol 11, ed C Domb and J L Lebowitz (London: Academic) p 55
[11] Burkhardt T W and Eisenriegler E 1985 *J. Phys. A: Math. Gen.* **18** L83
[12] Hanke A, Krech M, Schlesener F and Dietrich S 1999 *Phys. Rev.* E **60** 5163
[13] Cardy J L 1987 *Nucl. Phys.* B **290** 355
[14] Mc Avity D M and Osborn H 1995 *Nucl. Phys.* B **455** 522
[15] Burkhardt T W and Xue T 1991 *Phys. Rev. Lett.* **66** 895
    Burkhardt T W and Xue T 1991 *Nucl. Phys.* B **354** 653
    Burkhardt T W and Guim I 1987 *Phys. Rev.* B **36** 2080
    Burkhardt T W and Guim I 1993 *Phys. Rev.* B **47** 14306
[16] Brown L S 1980 *Ann. Phys.* **126** 135
    Brown L S and Collins J C 1980 *Ann. Phys.* **130** 215
[17] Cardy J L 1983 *J. Phys. A: Math. Gen.* **16** 3617